Efficient Self-Consistent Viscous-Inviscid Solutions for Unsteady Transonic Flow

James T. Howlett*
NASA Langley Research Center, Hampton, Virginia

An improved method is presented for coupling a boundary-layer code with an unsteady inviscid transonic computer code in a quasisteady fashion. At each fixed time step, the boundary layer and inviscid equations are successively solved until the process converges. An explicit coupling of the equations that greatly accelerates the convergence process is described. The computer times for converged viscous-inviscid solutions are about 1.8 times the comparable inviscid values. Comparisons of the results obtained with experimental data on three airfoils are presented. These comparisons demonstrate that the explicitly coupled viscous-inviscid solutions can provide efficient predictions of the pressure distributions and lift for unsteady two-dimensional transonic flows.

Nomenclature

CT	= computational test case
C_{ℓ_α}	= first harmonic lift coefficient due to pitch
C_{m_α}	= first harmonic pitching moment coefficient due to pitch
C_p	= pressure coefficient
C_E	= entrainment coefficient
c	= airfoil chord
F	= airfoil surface function
F_1F_2	= boundary-layer function, Eq. (7)
$\bar{H}$	= boundary-layer shape factor
k	= reduced frequency, $wc/2U$
M	= freestream Mach number
t	= time
U	= freestream velocity
x	= streamwise coordinate relative to leading edge
y	= coordinate normal to freestream, positive up
$\Delta(...)$	= indicates jump in ...
α_0	= mean angle of attack
α_1	= dynamic pitch angle
γ	= ratio of specific heats
γ^*	$= \gamma^* = 2-(2-\gamma)M^2$
δ	= airfoil thickness ratio
δ^*	= boundary-layer displacement thickness
θ	= boundary-layer momentum thickness
ϕ	= inviscid perturbation velocity potential
ϕV	= perturbation velocity potential with viscous interaction
ω	= angular frequency

Introduction

THE importance of viscous effects in accurate predictions of steady and unsteady transonic aerodynamic loading is well-known.[1] While Navier-Stokes computer codes can provide solutions[2] that include viscosity, their cost is prohibitive for routine use. As a result, extensive efforts are underway by various researchers to account for unsteady viscous effects by coupling a viscous boundary-layer model with an otherwise inviscid analysis.[3-6] As commonly implemented, the inviscid outer flow solution provides the surface pressure distribution needed to solve the boundary-layer equations. This yields the boundary-layer thickness distribution, which is used to modify the airfoil surface tangency boundary condition for the next iteration of the outer inviscid flow solution.

For steady flow problems, it has been demonstrated that this direct solution technique converges to consistent solutions of the boundary-layer and inviscid equations which show good agreement with experiments.[7] These converged interactive solutions are referred to as self-consistent solutions. For unsteady flow problems, these iterative solution techniques are impractical due to the high computational expense associated with a large number of iterations.

Rizzetta[1] coupled the steady integral lag entrainment boundary-layer model of Green[8] with the LTRAN2[9] unsteady transonic code in a quasisteady manner using a noniterative implicit technique. Guruswamy and Goorjian[3] applied the method of Rizzetta in a study of viscous effects on oscillating airfoils with the result that up to 8000 time steps per cycle were required to obtain reasonably accurate answers. For step sizes even smaller than this, the computer code became unstable. An alternative procedure of the noniterative type was reported by Houwink,[4] who used an explicit method of viscous-inviscid coupling and obtained satisfactory solutions with 120 time steps per cycle and computer times 30% higher than in the inviscid cases.

The present study began by incorporating Rizzetta's[1] boundary-layer algorithm into the XTRAN2L code.[10] Several changes were subsequently made to this procedure. The accuracy of the calculations was improved by incorporating an iterative viscous-inviscid solution at each time step. The convergence of the iterative solution was enhanced by the use of an explicit boundary-layer coupling. This paper discusses the modifications that have been made to the computational algorithm and presents comparisons of the results with experimental data on three airfoils.

Analysis

The inviscid code used in this study is the XTRAN2L computer code described by Whitlow.[10] This code is a modified version of the LTRAN2 code developed by Ballhaus and Goorjian.[9] The XTRAN2L code solves the complete two-

Presented as Paper 85-0482 at the AIAA 23rd Aerospace Sciences Meeting, Reno, NV, Jan. 14-17, 1985; received April 30, 1985; revision received Feb. 17, 1987.

*Aerospace Technologist, Loads and Aeroelasticity Division, Unsteady Aerodynamics Branch. Member AIAA.

dimensional transonic small disturbance (TSD) equation given by Eq. (1) and includes nonreflecting far-field boundary conditions:

$$\frac{4k^2M^2}{\delta^{2/3}}\phi_{tt}+\frac{4kM^2}{\delta^{2/3}}\phi_{xt}=[(1-M^2)/\delta^{2/3} -M^2(\gamma^*+1)\phi_x]\phi_{xx}+\phi_{yy} \quad (1)$$

The disturbance velocity potential ϕ is normalized by $cU\delta^{2/3}$ where c is the airfoil chord, δ is the airfoil thickness ratio, and U is the freestream speed. The spatial coordinates x and y and the time t are normalized by c, $c/\delta^{1/3}$, and ω^{-1} respectively, where ω is the frequency of unsteady motion. The reduced frequency (based on semichord) $k=\omega c/2U$, M is the freestream Mach number, and $\gamma^*=2-(2-\gamma)M^2$ where γ is the ratio of specific heats. The boundary conditions on the airfoil and wake for the inviscid code are

$$\text{airfoil: } \phi_y^{\pm}=F_x^{\pm}+F_t^{\pm} \quad (2)$$

$$\text{wake: } \Delta\phi_y=0 \quad (3)$$

$$\Delta(\phi_x+\phi_t)=0 \quad (4)$$

where the $\pm$ refers to the airfoil upper or lower surface, the function $F(x,t)$ denotes the airfoil surface, and $\Delta(...)$ indicates a jump in the bracketed quantity.

To account for the viscous boundary layer in a quasisteady manner, Eqs. (2) and (3) are modified as follows (see Houwink[5] and Rizzetta[1]):

$$\text{airfoil: } \phi_y^{\pm}=F_x^{\pm}+F_t^{\pm}+\left(\frac{\delta^*}{\delta c}\right)_x^{\pm} \quad (5)$$

$$\text{wake: } \Delta(\phi_y)=\Delta\left(\frac{\delta^*}{\delta c}\right)_x \quad (6)$$

where δ^* is the boundary-layer displacement thickness determined from Green's lag entrainment equations.

Equation (5) is a direct extension of the airfoil boundary condition as given by Rizzetta[1] to include the term $F_t^{\pm}$ which accounts for the time dependence of the airfoil motion in the boundary conditions. Note that although Eq. (5) is a commonly used form for analytically describing the inclusion of the boundary-layer equations, the precise manner in which this equation is incorporated into the computational algorithm can be a key feature of the efficiency and accuracy of the method (see Ref. 11, for example). This feature is discussed further in the following section.

The displacement thickness δ^* is computed as a function of the boundary-layer shape factor $\bar{H}$ and the momentum thickness θ, which are determined, together with the entrainment coefficient C_E, from Green's lag entrainment equations:

$$\theta_x=f_1+f_2\phi_{xx}$$

$$\bar{H}_x=f_3+f_4\phi_{xx}$$

$$(C_E)_x=f_5+f_6\phi_{xx}$$

where the coefficients f_1–f_6 are functions of θ, $\bar{H}$, C_E, and other parameters described in detail in Refs. 1 and 8.

Viscous Calculation Procedure

A key feature of any viscous-inviscid interaction method is the precise manner in which the boundary-layer calculations are coupled with the inviscid code. Several significant modifications of the procedures used by Rizzetta[1] have been incorporated into the present code, and these modifications are described in the following paragraphs.

1) The primary improvement in the algorithm is the incorporation of viscous-inviscid iterations at each time step. The effect of these iterations can be seen by considering the numerical implementation of the airfoil boundary conditions. In Rizzetta's analysis,[1] the last term on the right of Eq. (5) is implemented as

$$\left(\frac{\delta^*}{\delta c}\right)_x \approx F_1+F_2\phi_{xx}\approx F_1+\frac{2F_2}{x_{i+1}-x_{i-1}} \cdot\left[\left(\frac{\phi^n_{i+1,J}-\phi^{n+1}_{i,J}}{x_{i+1}-x_i}\right)-\left(\frac{\phi^{n+1}_{i,J}-\phi^{n+1}_{i-1,J}}{x_i-x_{i-1}}\right)\right] \quad (7)$$

where F_1 and F_2 are functions described in Ref. 1. Now $\phi^n_{i+1,J}$ and $\phi^{n+1}_{i,J}$ in this equation implicitly couple the two time levels n and $n+1$ at the two streamwise stations x_{i+i} and x_i. In the present analysis, these implicit equations are iterated at each time step.

Figure 1a presents a flow chart that describes the iteration procedure. For $t=t_{n+1}$, the boundary-layer functions F_1 and F_2 are calculated using the potential solution ϕ^n from the previous time step. During the y-sweep those functions are used in Eq. (7) to implicitly couple the boundary layer with the inviscid outer flow. The resulting solution for the coupled potential is denoted by ϕV^{n+1}. This coupled solution, ϕV^{n+1}, is then used to recalculate the boundary-layer parameters, and the process is repeated. Most applications investigated have required 5–25 iterations for convergence.

2) The coupling between the viscous boundary layer and the inviscid code was made explicit in a form similar to the noniterative coupling used by Houwink.[4] The explicit coupling between the boundary layer and the inviscid solution on the airfoil (but not on the wake) is implemented by the

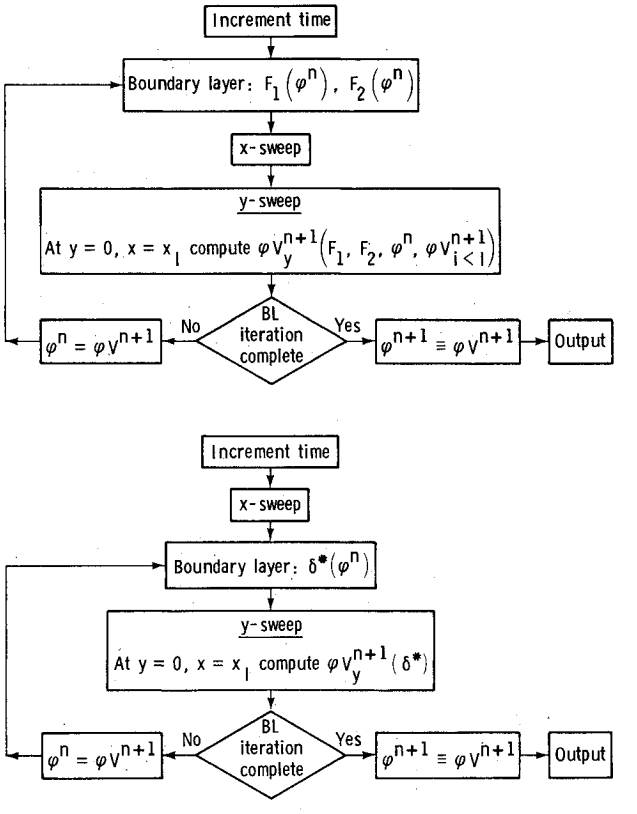

Fig. 1 Flow charts for boundary-layer coupling iterations: a) original viscous coupling and b) explicit viscous coupling.

direct use of Eq. (5) in the expression for the airfoil downwash. That is, at time level $t=t_{n+1}$, the last term on the right of Eq. (5) is evaluated by using values at the previous time step $t=t_n$ as follows:

$$\left(\frac{\delta^*}{\delta c}\right)_x = \frac{1}{\delta c}\left[\frac{\delta^{*n}_i - \delta^{*n}_{i-1}}{x_i - x_{i-1}}\right] \tag{8}$$

This procedure does involve a lag of boundary-layer displacement thickness by one time step, but it does not involve an implicit coupling between different time levels at different streamwise stations.

A flow chart indicating the explicit coupling algorithm is shown in Fig. 1b. As the figure indicates, the modifications for the explicit viscous coupling are included during the y-sweep of the alternating-direction-implicit (ADI) solution. The x-sweep calculations are identical for both forms of coupling. For computational efficiency, the self-consistent iterations are only done over the y-sweep. In practice, converged self-consistent solutions have been obtained in one iteration for most cases, resulting in more accurate viscous-inviscid solutions with reasonable computer times.

3) In the original algorithm, the viscous equations are integrated using a Runge-Kutta algorithm given the value of $(C_p)_x$ at each outer flow grid point on the airfoil and wake. The integration spatial step size was found to be too coarse, and a finer step size is used for the integration of the boundary-layer equations. Ten boundary-layer grid points are used between each pair of outer flow grid points. The required values of $(C_p)_x$ at the refined viscous grid points are determined by interpolation.

4) The empirical viscous wedge was eliminated, and the integration of the boundary-layer equations begins at a specified transition point. This allows a consistent description of the boundary layer from the specified transition point to the downstream boundary. Green's lag entrainment equations are simply integrated through the shock with no adverse effects. For results in this paper, transition is fixed at 10% chord unless stated otherwise.

5) Boundary-layer smoothing was introduced to reduce instabilities. The values of ϕ_x, ϕ_{xx} used in the boundary-layer calculations as well as the values of δ^* and δ^*_x are smoothed by averaging the values at 3-5 adjacent grid points.

Results and Discussion

Convergence Studies for Original Coupling

In order to test the validity of the self-consistent iteration procedure as described by modifications 1, 3, 4, and 5, extensive calculations have been performed on several airfoils. The results presented in this section are for the NACA 64A010 airfoil (theoretical section). This airfoil, at a Mach number of 0.78 and a one-degree angle of attack, has a moderately strong shock near midchord that is typical of the cases of interest. The results obtained for this airfoil are similar to the results obtained for the other airfoils studied.

The calculation procedure was as follows. Steady results for an inviscid analysis were calculated and used as a starting solution for a steady viscous solution. The steady viscous solution was then used as a starting solution for the unsteady viscous calculations. Unless otherwise stated, the unsteady results presented herein were run at 360 time steps per cycle, and transient effects were sufficiently damped out after two cycles to obtain the harmonic components by a Fourier analysis. The number of viscous iterations per time step was varied, and various unsteady quantities such as pressure, lift, and moment were compared as the number of iterations was increased. Comparisons with the results of Guruswamy and Goorjian[3] indicate that the effect of these iterations is closely equivalent to taking smaller time steps. That is, 360 time steps per cycle with two iterations per time step gives results similar to using 720 time steps per cycle. However, the iterative procedure does converge, as will be shown, whereas

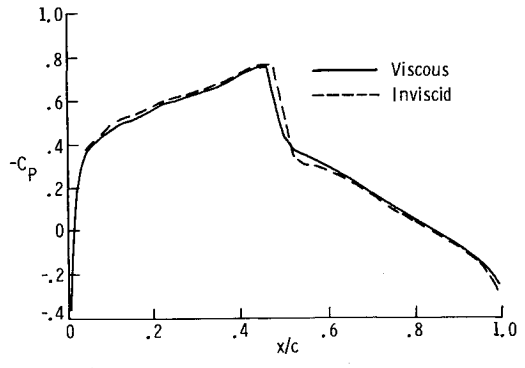

Fig. 2 Upper surface steady pressure for NACA 64A010 (theoretical) airfoil: original viscous coupling, $\alpha_0=1$ deg, $M=0.78$.

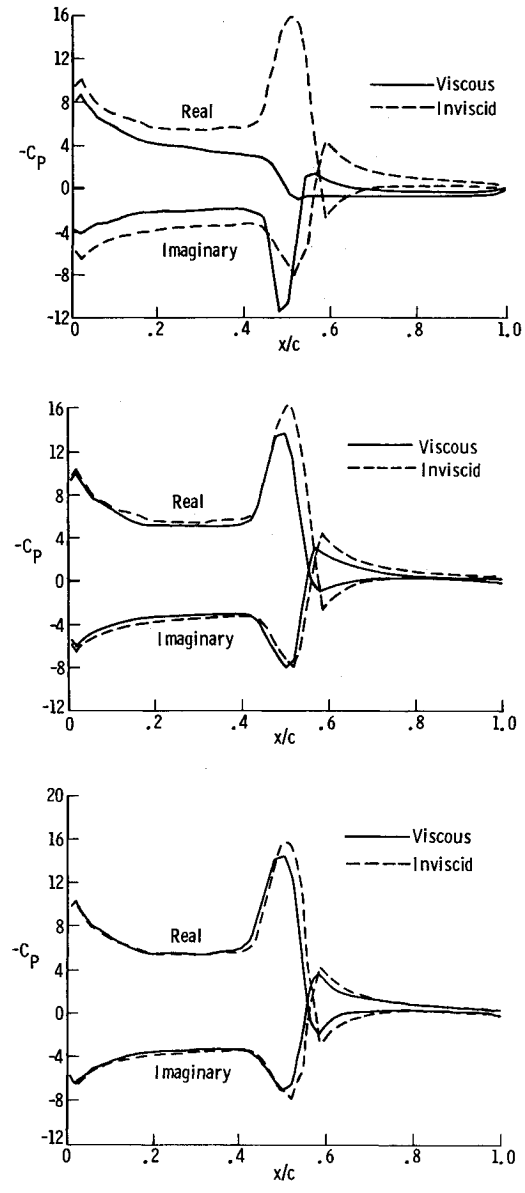

Fig. 3 Effect of number of viscous iterations for original viscous coupling method on upper surface unsteady pressure for NACA 64A010 (theoretical) airfoil: $\alpha_0=1$ deg, $\alpha_1=1$ deg, $M=0.78$, $k=0.1$: a) one viscous iteration, b) five viscous iterations, and c) 10 viscous iterations.

the use of successively smaller time steps can lead to stability problems.[3]

Figure 2 shows the pressure distributions on the airfoil upper surface for a steady flow at a one degree angle of attack and a 0.78 Mach number. As the figure indicates, a moderately strong shock is located near midchord with the viscous shock location slightly upstream of the inviscid shock.

The first harmonic components of the unsteady pressure distributions for a one degree oscillation in pitch ($\alpha_1 = 1$ deg) with $k = 0.1$ for varying numbers of iterations are shown in Fig. 3. For one iteration (Fig. 3a), the viscous solution is quite different from the inviscid solution. For five iterations (Fig. 3b), the viscous and inviscid solutions are nearly coincident except in the vicinity of the shock. Similar to results for the steady solution, the unsteady viscous solution has a somewhat weaker shock wave at a slightly upstream location. A comparison of Figs. 3b and 3c shows that the viscous solution after 10 iterations is nearly identical to the solution with five iterations, except for some minor differences in magnitude near the shock. This clearly demonstrates the importance of obtaining converged self-consistent solutions in assessing the effects of viscosity on pressure distributions.

Figure 4 shows the real and imaginary parts of the first harmonic component of the unsteady lift and moment as the number of iterations per time step is varied. For both lift and moment, the real part of the coefficient changes significantly as the number of iterations is increased from one to five, thereafter settling down and asymptotically approaching the converged value. The moment coefficient changes sign between the second and third iterations before asymptotically approaching the converged value. Since the moment coefficient is calculated about the quarter-chord for this case, some of this variation may be due to the sensitivity of the coefficient to small changes in the flow. Although not shown on this figure, calculations have been carried out for up to 22 iterations per time step, and the results were identical to those obtained for 10 iterations. The imaginary part of the unsteady lift changes very little during the iterations, whereas the trend for the imaginary part of the unsteady moment is quite similar to that of the real part. Also shown in the figure are the corresponding results for the inviscid analysis. The converged solution indicates that for this case the effects of viscosity are very minor and primarily result in a small reduction in the magnitude of both the unsteady lift and moment.

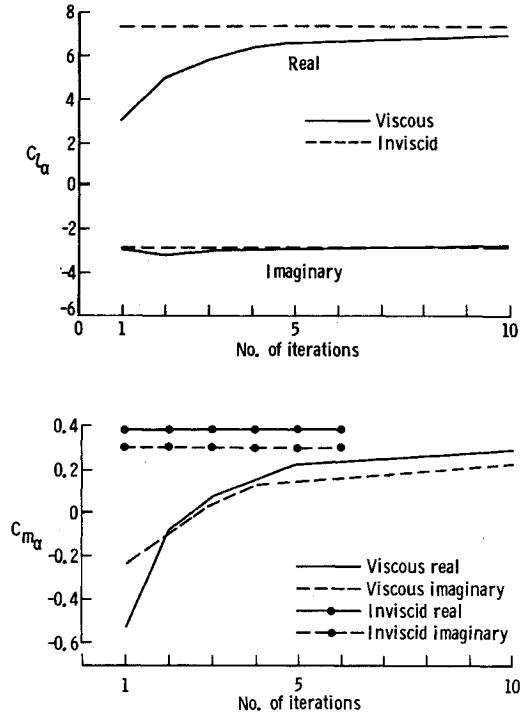

Fig. 4 Effect of number of viscous iterations for original viscous coupling method on unsteady forces for NACA 64A010 (theoretical) airfoil: $\alpha_0 = 1$ deg, $\alpha_1 = 1$ deg, $M = 0.78$, $k = 0.1$: a) unsteady lift and b) unsteady moment.

Explicit Coupling Studies

The computer costs associated with the large number of iterations required for converged self-consistent solutions with the original formulation of viscous-inviscid coupling is quite high. Each viscous iteration increases the computer time by about 80% of the inviscid solution time. A practical alternative for reducing the number of iterations has been found to be the explicit coupling between the inviscid equations and the boundary-layer displacement thickness described previously in modification 2. The explicitly coupled equations compute a self-consistent solution with very few iterations, usually just one. Hence, explicit coupling results in converged self-consistent solutions in computer times that are about 1.8 times the comparable inviscid values in many cases.

Figure 5 shows the first harmonic of the unsteady pressure distribution on the upper surface of the NACA 64A010 airfoil at a one degree angle of attack, a Mach number of 0.78, $\alpha_1 = 1$ deg, and $k = 0.1$ as computed using the explicit boundary-layer coupling. A comparison of Fig. 5a with Fig. 3c shows that the pressures obtained with one iteration of the explicit coupling are practically identical to those from the original coupling with 10 iterations. As shown by Fig. 5b, the results for 10 iterations with explicit coupling are the same as those obtained with one iteration, thus demonstrat-

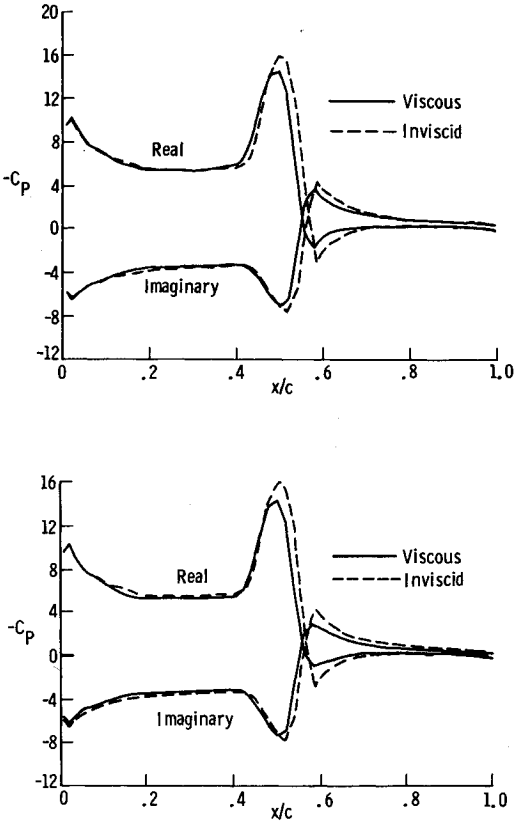

Fig. 5 Unsteady upper surface pressure with explicit viscous coupling compared with inviscid results for NACA 64A010 (theoretical) airfoil: $\alpha_0 = 1$ deg, $\alpha_1 = 1$ deg, $k = 0.1$: a) one viscous iteration and b) 10 viscous iterations.

ing that this solution is in fact a converged self-consistent solution.

Comparison with Experiments

In this section, calculations from the present analysis with the explicit viscous-inviscid coupling are compared with experimental data for several of the computational test cases selected by the AGARD Structures and Materials Panel[12] as well as with some published data for the MBB – A3 airfoil.[13] Additional information on the experimental configurations may be found in the references.[12,13]

NACA 64A010

The experimental results presented here are for the model tested at the NASA Ames Research Center and are taken from Chapter 2 of Ref. 12. Figure 6 shows the steady pressure distributions on the airfoil lower surface for the inviscid, viscous, and experimental results. The Mach number is 0.796 and the angle of attack is −0.21 deg. These steady results correspond to AGARD Computational Test (CT) case 5.[12] As with the previous results, the viscous effects are small. The predicted shock location for the viscous analysis is slightly forward of the inviscid shock location and agrees well with the experimental result. Downstream of the shock, both the viscous and inviscid analyses agree fairly well with the experiment.

Figure 7 presents the unsteady pressure distributions on the lower surface of the airfoil for AGARD CT case 5. The first harmonic components are compared with the experimental values for $\alpha_1 = 1$ deg and $k = 0.101$. The viscous shock pulse is about 2% chord upstream of the inviscid shock pulse and correlates better with the experimental values.

In Fig. 8, unsteady lift and moment coefficients vs frequency are presented. As shown in Fig. 8a, the viscous solution for the lift coefficient is closer to the experimental results than the inviscid solution and, for reduced frequencies greater than 0.1, agrees well with the experimental data. The calculated moment coefficients shown in Figs. 8b and 8c have the same trends as the experimental data for reduced frequencies greater than 0.1, although the actual values are significantly different. The source of this difference is unknown and further investigation is needed. The results do show that viscous effects are not the dominant effect in this difference.

For low but nonzero reduced frequencies, the results do deviate from the experimental values. As the figure shows, this problem also occurs in the inviscid code and is not due to the viscous modifications. This low-frequency discrepancy has been noted previously by other researchers.[14] For this

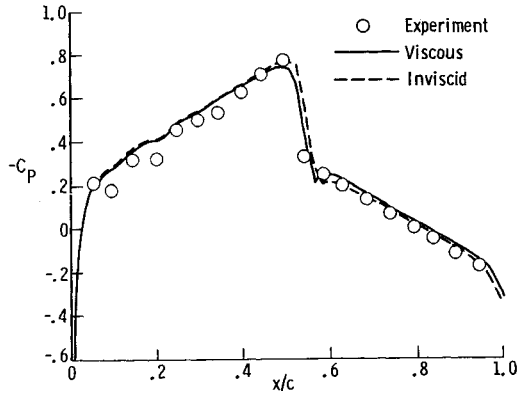

Fig. 6 Comparison between analytical and experimental steady pressure for lower surface of NACA 64A010 (experimental) airfoil: explicit viscous coupling, $\alpha_0 = -0.21$ deg, $M = 0.796$ (AGARD CT case 5).

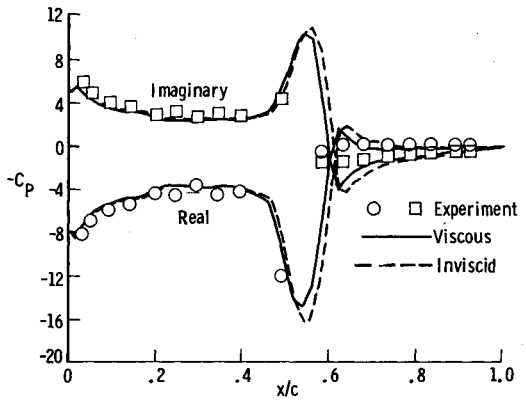

Fig. 7 Comparison between analytical and experimental unsteady pressure for lower surface of NACA 64A010 (experimental) airfoil: explicit viscous coupling, one iteration, $\alpha_0 = -0.21$ deg, $\alpha_1 = 1$ deg, $M = 0.796$, $k = 0.101$ (AGARD CT case 5).

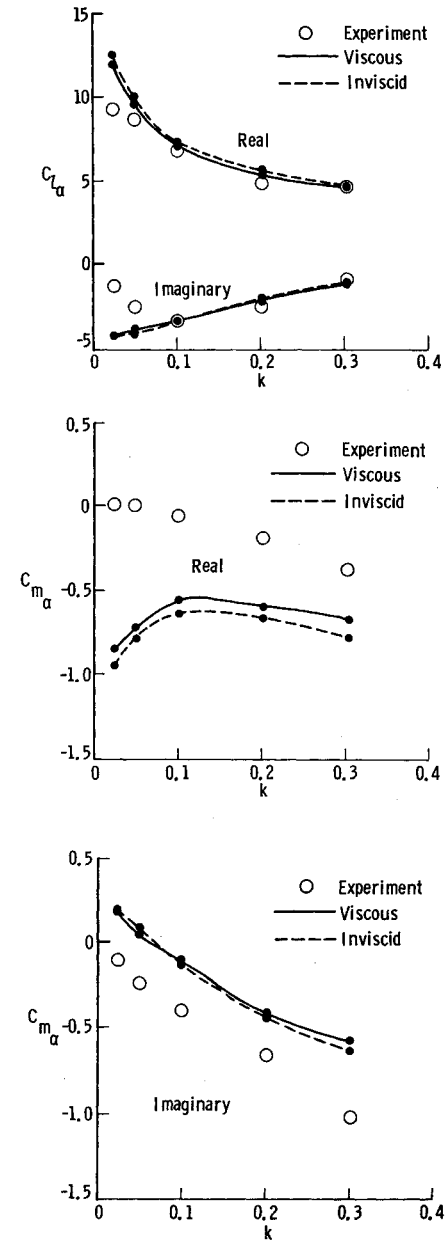

Fig. 8 Unsteady forces vs reduced frequency for NACA 64A010 (experimental) airfoil: a) unsteady lift, b) real part of unsteady moment, and c) imaginary part of unsteady moment.

airfoil, over the range of reduced frequencies investigated, the explicit coupling method provides efficient viscous predictions of the unsteady pressure distributions and lift coefficients which agree better with experiment than the inviscid results.

MBB-A3

The experimental pressure distribution for the supercritical MBB-A3 airfoil for a steady flow is taken from Ref. 13. Figure 9 presents comparisons of the steady pressure distributions for the experiment, the viscous and the inviscid analyses for the design condition of the airfoil. Note that the calculated values were obtained by using the actual experimental values for the Mach number and the angle of attack rather than values that have been adjusted to match flow conditions in the wind tunnel, as is frequently done in comparisons with this particular data. For the viscous solution, the shock is located about 4% chord forward of the inviscid shock location and is somewhat weaker. However, a large discrepancy between the experimental values and the viscous prediction still exists and further investigation is required.

Figure 10 presents the unsteady pressure distribution for the viscous and inviscid solutions for a reduced frequency of 0.1 and $\alpha_1 = 0.5$ deg. The results are analogous to those for the steady case. On the upper surface of the airfoil, the shock location for the viscous solution is about 5% chord forward of the inviscid shock location, and the shock strength for the viscous solution is considerably weaker than that of the inviscid solution. On the lower surface of the airfoil, the unsteady pressure distributions for both solutions are essentially the same.

NLR 7301

The experimental results for the supercritical NLR 7301 airfoil are taken from Chap. 4 of Ref. 12. The calculated results presented herein correspond to the test conditions for AGARD CT cases 3 and 5,[12] although some differences do exist between these values and actual wind tunnel test conditions. An excellent discussion of this point is given by Lambourne in Chapter 0 of Ref. 12.

It should be noted that the test cases investigated herein for this airfoil do fall within the region where the potential formulation may experience anomalous results related to nonuniqueness.[15] Some preliminary studies of the effects of the viscous boundary layer on the failure of potential theory are reported by Williams et al.[16] These authors conclude that this type of failure of potential theory is not cured by the inclusion of boundary-layer interactions.

Figure 11 presents the steady pressure distributions for the experimental and analytical cases with $M = 0.7$ and $\alpha_o = 2$ deg. These values correspond to the AGARD CT cases 3 and 5. For the viscous solution, transition is fixed at 30% chord to correspond to the experimental configuration.[12] The shock location for the inviscid solution is about 20% chord downstream of the experimental shock location. The viscous solution has a shock location and strength nearly coincident with the experimental result. On the airfoil lower surface, pressures from the viscous solution are slightly below the experimental values, although they agree better with the experiment than do the inviscid values. This close agreement between the experiment and the viscous solution for this difficult case may be somewhat fortuitous due to the previously mentioned differences between the parameters for the AGARD cases and the wind tunnel tests.

In Fig. 12, the unsteady pressure distributions are plotted corresponding to AGARD CT case 3 with $\alpha_1 = 0.5$ deg and $k = 0.072$. The unsteady viscous results for this airfoil were computed with 720 time steps per cycle and two viscous iterations (explicit coupling) per time step. As Fig. 12a shows, on the airfoil upper surface the viscous solution agrees much better with the experiment than does the inviscid solution. The viscous shock pulse is slightly downstream of the experimental location, significantly weaker and broader. As shown in Fig. 12b, on the airfoil lower surface viscous effects are small, and the agreement between the calculated results and the experiment is good.

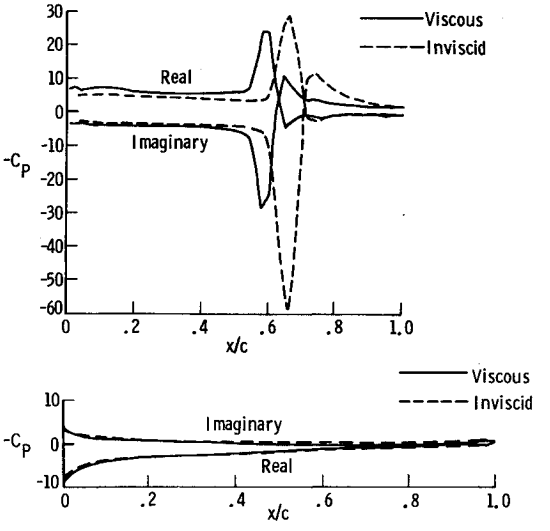

Fig. 10 Comparison of viscous and inviscid analytical unsteady pressure for supercritical MBB-A3 airfoil: explicit viscous coupling, $\alpha_0 = 1.5$ deg, $\alpha_1 = 0.5$ deg, $M = 0.765$, $k = 0.1$: a) upper surface pressure and b) lower surface pressure.

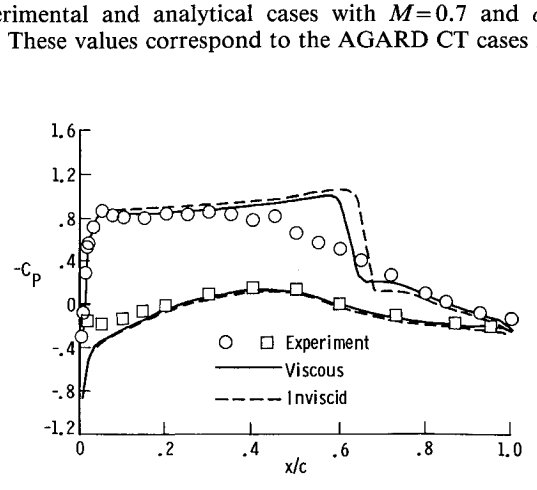

Fig. 9 Comparison of analytical and experimental steady pressure for supercritical MB-A3 airfoil: explicit viscous coupling, $\alpha_0 = 1.5$ deg, $M = 0.765$.

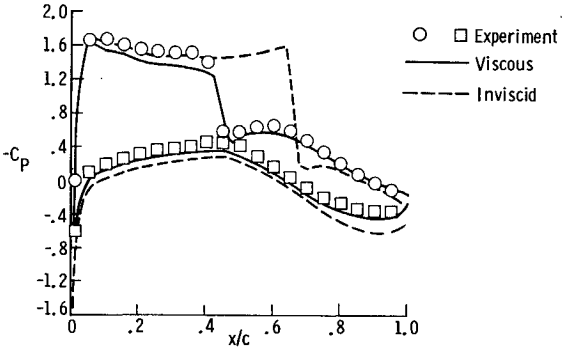

Fig. 11 Comparison of analytical and experimental steady pressure for supercritical NLR 7301 airfoil: explicit viscous coupling, $\alpha_0 = 2$ deg, $M = 0.7$ (AGARD CT cases 3 and 5).

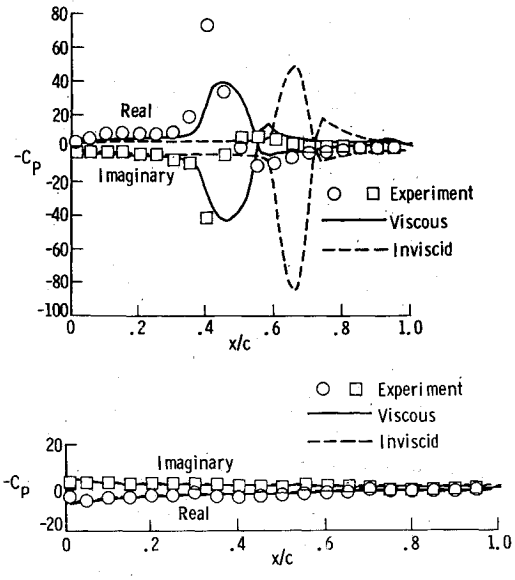

Fig. 12 Comparison of analytical and experimental unsteady pressure for supercritical NLR 7301 airfoil: explicit viscous coupling, two iterations, $\alpha_0 = 2$ deg, $\alpha_1 = 0.5$ deg, $M = 0.7$, $k = 0.072$ (AGARD CT case 3): a) upper surface pressure and b) lower surface pressure.

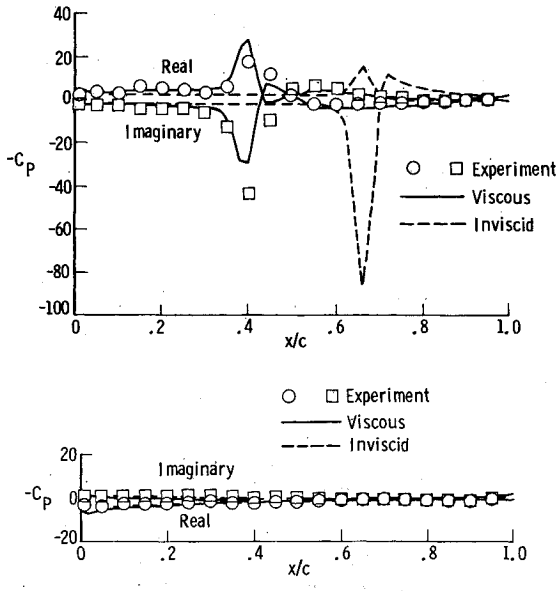

Fig. 13 Comparison of analytical and experimental unsteady pressure for supercritical NLR 7301 airfoil: explicit viscous coupling, two iterations, $\alpha_0 = 2$ deg, $\alpha_1 = 0.5$ deg, $M = 0.7$, $k = 0.192$ (AGARD CT case 5): a) upper surface pressure and b) lower surface pressure.

Figure 13 presents unsteady pressure distributions for a higher reduced frequency of $k = 0.192$ with $\alpha_1 = 0.5$ deg (AGARD CT case 5). As with the previous case, the viscous solution agrees quite well with the experiment, whereas the inviscid solution is considerably different. Figure 13a shows that the location of the viscous shock pulse is correctly predicted, although it is much narrower and some differences are noted in amplitude. On the airfoil lower surface, viscous effects are small, and the calculated results agree well with the experiment, as shown in Fig. 13b.

Conclusions

This paper has presented a study of self-consistent solutions for viscous-inviscid interactions in unsteady two-dimensional transonic flow. A self-consistent iterative procedure has been combined with two different numerical techniques for coupling the quasisteady viscous boundary layer with the inviscid solution: 1) the original method of Rizzetta,[1] and 2) the explicit coupling based upon the work of Houwink.[4] Both methods are based upon the two-dimensional XTRAN2L inviscid transonic computer code coupled with a turbulent viscous boundary layer represented by Green's lag entrainment equations. In this study, the viscous wedge in Rizzetta's analysis has been eliminated and the transition point is specified. Each method successively solves the boundary-layer and inviscid equations at each fixed time step until the process converges. The results demonstrate that both methods converge to self-consistent solutions. However, method 2, which incorporates explicitly coupled viscous-inviscid equations, computes a converged self-consistent solution in one or two iterations, whereas method 1 requires 5–25 iterations to converge. The computer code with explicitly coupled equations yields computer times that are reduced by a factor of 20 from those of method 1. Accurate, self-consistent, converged, viscous-inviscid solutions are obtained in computer times that are about 1.8 times the comparable inviscid values.

Comparisons of unsteady forces and pressure distributions computed with the original coupling method for various numbers of iterations have demonstrated the importance of obtaining converged self-consistent solutions for an accurate assessment of viscous effects. For the NACA 64010 (experimental) airfoil, unsteady lifting forces obtained by the viscous calculations with explicitly coupled boundary conditions agree well with experimental results for reduced frequencies greater than 0.1 over the range studied. Unsteady moment coefficients indicated the same trend as the experimental results, although the magnitudes were significantly different.

Comparisons of steady pressure distributions for the supercritical MBB-A3 airfoil show that the viscous shock location (explicit coupling) is about 4% chord forward of the inviscid shock location, although a large discrepancy still exists between the viscous results and the experiment. The source of this discrepancy is not known, and further investigation is required.

For the supercritical NLR 7301 airfoil, comparisons of the experimental results with viscous solutions computed by the explicitly coupled equations clearly demonstrate that this type of analysis can yield accurate predictions of both the steady and unsteady pressure distributions for this difficult case. Although some differences in shock strength do exist for the conditions investigated, both the steady and unsteady shock locations are predicted with good accuracy.

The results presented demonstrate that self-consistent viscous solutions computed with the explicit coupling algorithm can provide efficient predictions of the pressure distributions and lift for an unsteady transonic flow which correlate better, sometimes significantly better, with experimental values than do the inviscid solutions.

Acknowledgment

The author would like to express his appreciation to Dr. Peter Goorjian of the Applied Computational Fluids Branch, NASA Ames Research Center for providing the original viscous LTRAN2 code.

References

[1]Rizzetta, D.P., "Procedures for the Computation of Unsteady Transonic Flows Including Viscous Effects," NASA CR 166249, Jan. 1982.

[2]Chyu, W.J. and Ono, K., "Unsteady Transonic Flow Over Conventional and Supercritical Airfoils," AIAA Paper 83-0235, Jan. 1983.

[3]Guruswamy, P. and Goorjian, P.M., "Effects of Viscosity on Transonic Aerodynamic and Aeroelastic Characteristics of Oscillating Airfoils," AIAA Paper 83-0888, May 1983.

[4]Houwink, R., "Results of a New Version of the LTRAN2-NLR code (LTRAN-V) for Unsteady Viscous Transonic Flow Computations," NLR Rept. NLR TR 81078U, July 1981.

[5]Houwink, R. and Veldman, A.E.P., "Steady and Unsteady Separated Flow Computations for Transonic Airfoils," AIAA Paper 84-1608, June 1984.

[6]Rizzetta, D.P. and Borland, C.J., "Numerical Solution of Three-Dimensional Unsteady Transonic Flow Over Wings Including Inviscid/Viscous Interactions," NASA CR166561, Feb. 1984.

[7]Street, C.L., "Viscous-Inviscid Interaction for Transonic Wing-Body Configurations Including Wake Effects," *AIAA Journal,* Vol. 20, July 1982.

[8]Green, J.E., Weeks, D.J., and Brooman, J.W.F., "Prediction of Turbulent Boundary Layers and Wakes in Compressible Flow by a Lag-Entrainment Method," RAE Reports and Memoranda 3791, Jan. 1973.

[9]Ballhaus, W.F. and Goorjian, P.M., "Implicit Finite-Difference Computations of Unsteady Transonic Flows About Airfoils," *AIAA Journal,* Vol. 15, Dec. 1977.

[10]Whitlow, W. Jr., "XTRAN2L: A Program for Solving the General-Frequency Unsteady Transonic Small Disturbance Equation," NASA TM 85723, Nov. 1983.

[11]Melnik, R.E., "Turbulent Interactions on Airfoils at Transonic Speed—Recent Developments," *Computation of Viscous-Inviscid Interactions,* AGARD CP 291, Feb. 1981.

[12]Anon., "Compendium of Unsteady Aerodynamic Measurements," AGARD Rept. 702, Aug. 1982.

[13]Bucciantini, G., Oggiano, M.S., and Onorato, M., "Supercritical Airfoil MBB-A3 Surface Pressure Distributions, Wake and Boundary Condition Measurements," *Experimental Data Base for Computer Program Assessment,* AGARD Advisory Rept. 138, May 1979.

[14]Edwards, J.W., Bland, S.R., and Seidel, D.A., "Experience with Transonic Unsteady Aerodynamic Calculations," NASA TM 86278, Aug. 1984.

[15]Salas, M.D. and Gumbert, C.R., "Breakdown of the Conservative Potential Equation," AIAA Paper 85-0367, Jan. 1985.

[16]Williams, M.H., Bland, S.R., and Edwards, J.W., "Flow Instabilities in Transonic Small-Disturbance Theory," *AIAA Journal,* Vol. 23, Oct. 1985.